JOURNAL OF AIRCRAFT
Vol. 45, No. 4, July–August 2008

# Landing Gear Influence on the Wake Vortex of a Large Transport Aircraft

Alexander Allen* and Christian Breitsamter†
*Technical University of Munich, 85747 Garching, Germany*

DOI: 10.2514/1.34995

**An experimental investigation on the wake vortex formation and evolution of a four-engine large transport aircraft model in the near field and extended near field has been conducted by means of hot-wire anemometry in a wind tunnel. The half-model used has a scale of 1:19.25 and the tests focus on the high-lift case of a typical landing configuration at a Reynolds number of $0.52 \times 10^6$ based on the wing mean aerodynamic chord. The flowfield is investigated up to 4.7 spans downstream of the model, which is investigated with and without landing gear. Based on the measured time-dependent velocity components, the wake flowfield is analyzed by distributions of vorticity, turbulence intensities, and spectral densities. The landing gear consists of a stay and four wheels, which create a bluff-body wake that interferes with the shear layer caused by the wing and wing junction. The landing gear creates a low-energy vortex system and a highly turbulent wake. Due to the landing gear, the main vortex centers are located slightly further outboard and the roll-up process is retarded, especially the inboard movement of the horizontal tail plane vortex. The velocity spectra of the landing gear wake show broadband characteristics with some moderate narrowband energy concentrations in the close near field, which do not enhance inherent wake instabilities. Although the turbulence caused by the landing gear is still present in the extended near field, only a small influence on the overall vortex system of the entire aircraft can be found. The landing gear influence is therefore negligible in the context of reducing minimum aircraft separation distances.**

## Nomenclature

| | | |
|---|---|---|
| AR | = | aspect ratio |
| $b$ | = | wing span, m |
| $C_L$ | = | lift coefficient, $2L\mathrm{AR}/(\rho U_\infty^2 b^2)$ |
| $f$ | = | frequency, Hz |
| $k$ | = | reduced frequency, $fb/(2U_\infty)$ |
| $L$ | = | lift, N |
| $l_\mu$ | = | wing mean aerodynamic chord, m |
| $Re_{l_\mu}$ | = | Reynolds number, $U_\infty l_\mu/\nu$ |
| $S_{u'}^N$ | = | power spectral density of $u'$ normalized with $(\Delta k U_\infty)/(\overline{u'^2}(b/2))$ |
| $Tu_y$ | = | lateral turbulence intensity, $\sqrt{\overline{v'^2}}/U_\infty$ |
| $U_\infty$ | = | freestream velocity, m/s |
| $u, v, w$ | = | axial, lateral, and vertical velocities, m/s |
| $\bar{u}, \bar{v}, \bar{w}$ | = | mean axial, lateral, and vertical velocities, m/s |
| $u', v', w'$ | = | fluctuation part of $u$, $v$, and $w$, m/s |
| $x, y, z$ | = | coordinates in the $x$, $y$, and $z$ directions, m |
| $x^*$ | = | nondimensional distance in the $x$ direction, $x/b$ |
| $y^*, z^*$ | = | nondimensional distances in the $y$ and $z$ directions, $2y/b$, $2z/b$ |
| $\alpha$ | = | aircraft angle of attack, deg |
| $\nu$ | = | kinematic viscosity, $\mathrm{m}^2/\mathrm{s}$ |
| $\xi$ | = | nondimensional axial vorticity, $\bar{\omega}_x b/(2U_\infty)$ |
| $\rho$ | = | density, $\mathrm{kg}/\mathrm{m}^3$ |
| $\tau^*$ | = | nondimensional time, $x^* 16 C_L/(\pi^4 \mathrm{AR})$ |
| $\bar{\omega}_x$ | = | mean axial vorticity component, $(\mathrm{d}\bar{w}/\mathrm{d}y - \mathrm{d}\bar{v}/\mathrm{d}z)$, 1/s |

Received 5 October 2007; revision received 12 November 2007; accepted for publication 13 November 2007. 

*Dipl.-Ing., M.Sc., Research Engineer, Institute of Aerodynamics. Member AIAA.

†PD Dr.-Ing., Chief Scientist, Institute of Aerodynamics. Associate Fellow AIAA.

## Introduction

THE flight safety of an aircraft may be endangered by encountering the wake vortices emanating from preceding large transport aircraft. The trailing wake of a lifting body rolls up into a pair of strong counter-rotating longitudinal vortices that persist for many body dimensions downstream [1–4]. A sudden upwash, downwash, or rolling, along with increased structural dynamic loads, can be experienced by an aircraft encountering a vortex wake, depending on its position and orientation with respect to the wake. Maintaining a suitably large spacing between the aircraft during takeoff and landing, as well as on flight routes, currently ensures flight safety. These separation distances are regulated by the Federal Aviation Administration in the U.S. and by the Civil Aviation Authority in Europe [5]. These distances are often considered as conservative because they do not account for the varying behavior of the vortices under different atmospheric conditions. Because of the severe increase in air traffic, many major airports will experience their limitations, leading to a critical assessment of aircraft spacing, especially for takeoff and landing.

In the past, numerous experimental and numerical investigations have been performed on the wake structure of generic wing configurations (EuroWake [6], C-Wake [7], and AWIATOR [8]). Alleviating the wake vortex hazard by modifications of wing geometry and/or wing loading is the aim of many research activities. Strategies to minimize the wake vortex hazard concentrate either on a quickly decaying vortex (QDV) or on a low-vorticity vortex (LVV) design. Promoting three-dimensional instabilities by means of active or passive devices may enhance vortex decay (QDV) [9,10]. The LVV design reduces the wake vortex hazard by enhancing the diffusion of the vorticity field. It is aimed at the generation of wake vortices with a larger core size and smaller swirl velocities at the core radius after roll-up is completed. Injecting additional turbulence into the wake and/or altering the circulation distribution of the wake-generating wing may lead to an increase of the dispersion of vorticity. The first type of mechanism is related to the use of spoilers or wing fins, and the second type of mechanism is related to differential flap setting.

The deployed landing gear, triggering a mechanism similar to a spoiler, also cause a significant turbulent wake, which may affect the wake vortex roll-up and the spatial vorticity distribution. Thus, deploying the landing gear earlier in the approach phase without

reducing the initial approach speed may result in weaker trailing vortices and therewith a reduced aircraft spacing. Of course, this measure cannot be applied for the takeoff and climb phase, but the duration of the approach phase in comparison is much longer. Therefore, the influence of the landing gear on the wake vortex formation and evolution in the near field and extended near field of a typical four-engine large transport aircraft (LTA) model in landing configuration is experimentally investigated here [11]. To the authors' knowledge, numerical and flight test data on the influence of a landing gear on the wake vortex system are not available. The results are obtained within the European community's Specific Targeted Research Project "FAR-Wake" (Fundamental Research on Aircraft Wake Phenomena). To obtain precise information on the near-field wake vortex structure, the present investigation focuses on the vorticity and turbulence content, comparing the cases with and without deployed landing gear.

## Experimental Setup

The investigation was conducted in the wind-tunnel facility C of the Institute of Aerodynamics at the Technical University of Munich, using a detailed large transport aircraft configuration and employing advanced hot-wire anemometry.

The wind tunnel C is a closed-return type and has a long-range test section of 21 m length, which covers a wake distance of approximately 4.7 spans downstream of the model. The wind tunnel has a cross section of $1.8 \times 2.7$ m.

A 1:19.25 scaled half-model of a typical large transport aircraft is used (Fig. 1a). The model has a wing semispan of 1.491 m ($AR = 10.1$), a wing mean aerodynamic chord of 0.357 m, and a fuselage length of 2.907 m. The model is made of steel and is equipped with fully adjustable flaps, slats, ailerons, and a horizontal tail plane. The experiments concentrate on the landing configuration with a typical setting of the high-lift devices. The outboard and midboard slats are set to 23.0 deg, and the inboard one is deflected to 19.6 deg. The inboard and outboard flaps are extended to 26.0 deg and the ailerons (inboard and outboard) are adjusted to 5 deg. To achieve a setting corresponding to straight and level flight, in which the pitching moment is zero, the horizontal tail plane is set to −6.0 deg. The engine nacelles are designed as throughflow nacelles. The model is investigated for the cases without (baseline) and with main landing gear (Fig. 1b).

A triple-wire probe operated by a multichannel constant-temperature anemometer system is used to measure the time series of axial, lateral, and vertical velocities. The tungsten wires are platinum-plated and have a diameter of 5 $\mu$m and a length of approximately 1.25 mm. The wires are arranged perpendicularly to each other to achieve best angular resolution. An additional temperature probe is employed to correct anemometer output voltages if ambient flow temperature varies. A sampling rate of 3000 Hz (Nyquist frequency 1500 Hz), a low-pass filter frequency of 1000 Hz, and a sampling time of 6.4 s were chosen. The sampling time corresponds to 19,200 values per wire and survey point. The signals are digitized with 16-bit precision through a 16-channel simultaneous-sampling A/D converter. The sampling parameters were achieved by preliminary tests to ensure that all relevant flowfield phenomena are detected. The anemometer output signals are converted into time-dependent velocity components $u$, $v$, and $w$ using a look-up table previously obtained from the velocity- and angle-dependent calibration of the hot-wire probe [12]. Data accuracy and repeatability, respectively, are judged on statistical error analysis, taking into account the characteristics of the signal processing equipment and the look-up table procedure used. Based on random error evaluation, accuracies are in the range of 1% for mean quantities, 2.5% for rms quantities (turbulence intensities), and 4% for spectral densities [13].

The investigations are all performed at a velocity of $U_\infty = 25$ m/s, corresponding to a Reynolds number of $Re_{l_\mu} = 0.52 \times 10^6$ based on the wing mean aerodynamic chord, which is an order of magnitude below the flight Reynolds number. Transition strips were attached to the model, and inspecting the surface flow

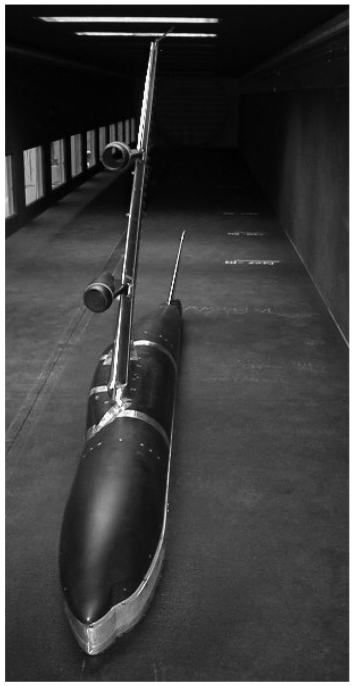

a)

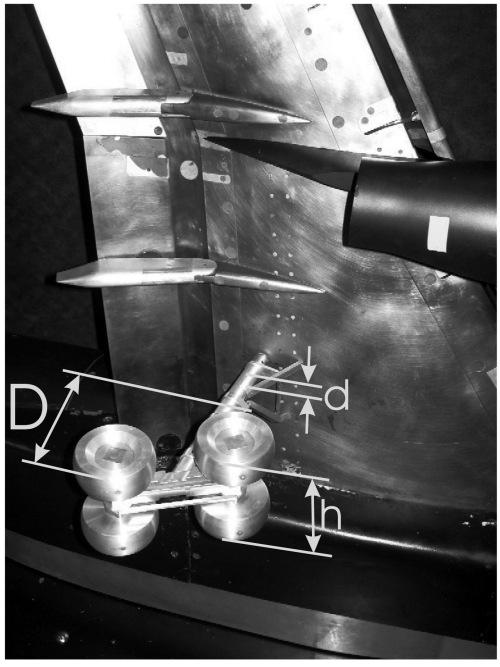


b)

**Fig. 1 Investigated configurations: a) baseline and b) with landing gear.**

with tufts showed that attached flow is present on the wing and horizontal tail plane. The angle of attack is chosen to be $\alpha = 7.0$ deg, which corresponds to a lift coefficient of $C_L = 1.43$, which is significantly below $C_{L,\max}$. Taking these aspects into account, the Reynolds number influence on the wake vortex roll-up process is small [14].

The model is positioned on the tunnel floor, with the wing reference point (WRP) at 2.8 m downstream of the nozzle exit and the wing tip pointing upward. The WRP is the position of the trailing edge at the winglet tip at an angle of attack of $\alpha = 0.0$ deg. A peniche with a height of 0.095 m is used to raise the model fuselage above the wind-tunnel-floor boundary layer. The test section is equipped with a

three-axis-probe traversing system. The vortex wake is measured in seven crossflow planes orientated perpendicularly to the freestream direction at distances $x^* = x/b = 0.02$, 0.37, 1.0, 2.0, 3.0, 4.0, and 4.7 downstream of the WRP. In regions of high flow gradients (i.e., in the areas of vorticity layers and vortex cores), the survey points are closely spaced, with a relative grid resolution of 0.007 in the spanwise and 0.010 in the vertical directions, based on the wing span. Outside these regions, the relative spacing is gradually enlarged to 0.040 laterally and 0.060 vertically. Regarding the susceptibility of vortical structures to intrusive measurements, it was found that the presence of the hot-wire probe has no marked influence on the wake vortex formation and evolution [9].

## Results and Discussion

For the configuration with landing gear, axial vorticity and lateral turbulence intensity fields are investigated for a station close to the wing trailing edge at $x^* = 0.02$ and $\tau^* = 0.0005$ (Fig. 2). Four main vortices can be identified: namely, from outboard to inboard, the outboard nacelle vortex (ONV), the outboard flap vortex (OFV), the inboard nacelle vortex (INV), and the landing gear vortex system (Fig. 2a). The wing tip vortex (WTV) is not clearly visible in this plane, because the used probe mount does not reach that far. Because of the presence of the fuselage, it is not possible to measure at positions $y^* < 0.144$, which is why the wing–fuselage vortex (WFV) is not depicted. The measuring plane is upstream of the horizontal tail plane, and thus the horizontal tail plane vortex (HTV) is also not present in Fig. 2. The vortex sheet emanating from the wing trailing edge with the dominating vortices embedded is clearly shown. Also, several less pronounced vortices, indicated by smaller vorticity levels, are present between the dominating wing vortices. These smaller vortices are caused by slat horns, flap track fairings, and other geometric discontinuities of the wing. Figure 2b shows local turbulence maxima in the regions of high vorticity. A turbulence bubble at the inner edge of the measuring plane is visible, which is caused by the deployed landing gear. The upper part of the bubble emanates from the inclined front wheel pair and the lower part emanates from the rear pair, which is positioned lower in respect to the front pair. Slightly outboard therefrom is the turbulence caused by the inboard nacelle, and at approximately $y^* = 0.7$, the turbulence caused by the outboard nacelle is visible.

At $x^* = 0.37$ and $\tau^* = 0.009$, the WTV and HTV are also depicted for the baseline configuration (Fig. 3a). For the configuration with landing gear, the WFV is additionally visible. Because of different probe mounts used for the two configurations,

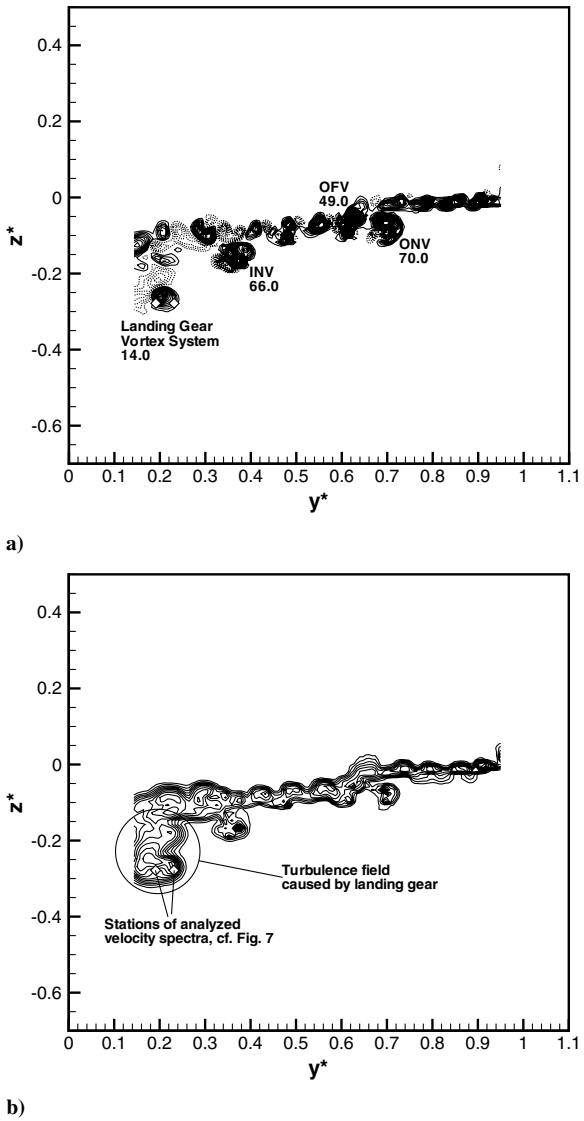


**Fig. 2 Contour plots of nondimensional axial vorticity $\xi$ and turbulence intensity $Tu_y$ distributions for the configuration with landing gear at $x^* = 0.02$ and $Re_{l_\mu} = 0.52 \times 10^6$ for a) $\xi$ ($-20 \le \xi \le 50$ and $\Delta\xi = 1$) and b) $Tu_y$ ($0.02 \le Tu_y \le 0.2$ and $\Delta Tu_y = 0.01$); solid lines are positive values and dashed lines are negative values.**

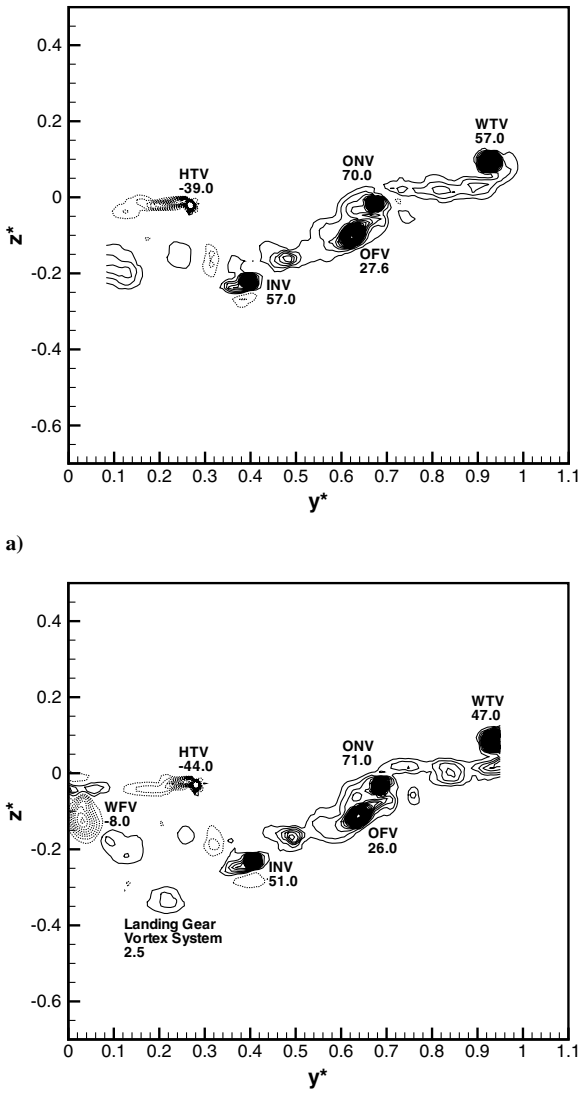


**Fig. 3 Contour plots of nondimensional axial vorticity $\xi$ distributions at $x^* = 0.37$ and $Re_{l_\mu} = 0.52 \times 10^6$ ($-20 \le \xi \le 50$ and $\Delta\xi = 1$) for the a) baseline configuration and b) configuration with landing gear; solid lines are positive values and dashed lines are negative values.**

different parts of the flowfield are visible; that is, for the baseline, the part $0.08 < y^* < 1.05$ was measured, and for the configuration with landing gear, $0.0 < y^* < 0.95$ was of higher interest. Further flowfield data were measured at $x^* = 1.0$, 2.0, 3.0, and 4.0, the data of which are documented in [11]. Downstream from $x^* = 1.0$, all dominant vortices are entirely located within the measurement plane. Note that the HTV and the WFV have negative vorticity and are therefore counter-rotating in comparison with the other five vortices. The horizontal tail plane is adjusted for negative lift due to trimmed flight, and therefore the HTV exhibits negative vorticity. The negative circulation gradient in the wing–fuselage region leads to the WFV, thus also characterized by negative axial vorticity. Further, the vortex sheet shed at the horizontal tail plane, which has not yet rolled up into the HTV, is clearly shown. The entire vorticity region has moved downward in comparison with $x^* = 0.02$, due to the downwash caused by the lift-producing wing. The peak vorticity values of the dominating vortices do not differ significantly in comparison with the baseline configuration. For the configuration with landing gear, the HTV is positioned further outboard. The other vortices only show a minor outboard displacement.

The shear layer from the wing is observable with the higher turbulence intensities, indicating the vortices (Fig. 4). The kink in the shear layer between $y^* = 0.6$ and 0.7 corresponds to the position of the outer flap edge. Further outboard on the wing, the ailerons are positioned at +5 deg, causing only a small downwash of the shear layer, whereas inboard, the flaps are positioned at +26 deg, causing a larger downwash, and hence a kink in the shear layer results. The bubble at $y^* = 0.4$ indicates the INV caused by the inboard nacelle, which is positioned below the wing. The fuselage wake is visible by a large region of increased turbulence intensity close to the plane of symmetry ($y^* \approx 0$ and $-0.25 < z^* < 0.05$). At $0.12 < y^* < 0.25$ and $-0.1 < z^* < -0.3$, a significant difference can be found between the baseline configuration (Fig. 4a) and the configuration with landing gear (Fig. 4b). This is again caused by the inclined landing gear wheel pairs.

Moving downstream, all vortices rotate counterclockwise around the roll-up center ($y^* \cong 0.73$) and the shear layers roll up into the corresponding vortices. The turbulence emanating from the landing gear merges with the turbulence from the fuselage at approximately $x^* = 2.0$.

At $x^* = 4.7$ ($\tau^* = 0.105$), the vortices have almost turned 135 deg around their roll-up center. Figure 5a still clearly shows the WTV, ONV/OFV, and INV. Vorticity intensities have decreased. For the configuration with landing gear, the HTV is positioned further outboard, caused by the additional turbulence emanated by the landing gear (Fig. 6b). In this figure, the additional turbulence caused

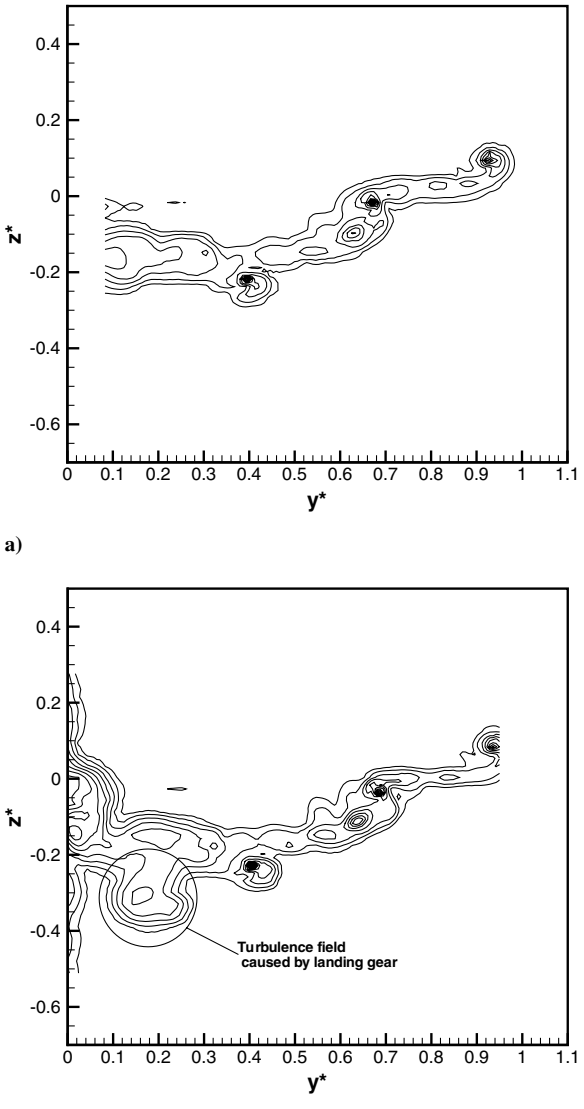


a)

b)

**Fig. 4 Contour plots of turbulence intensity $Tu_y$ distributions at $x^* = 0.37$ and $Re_{l_u} = 0.52 \times 10^6$ ($0.02 \le Tu_y \le 0.2$ and $\Delta Tu_y = 0.01$) for the a) baseline configuration and b) configuration with landing gear.**

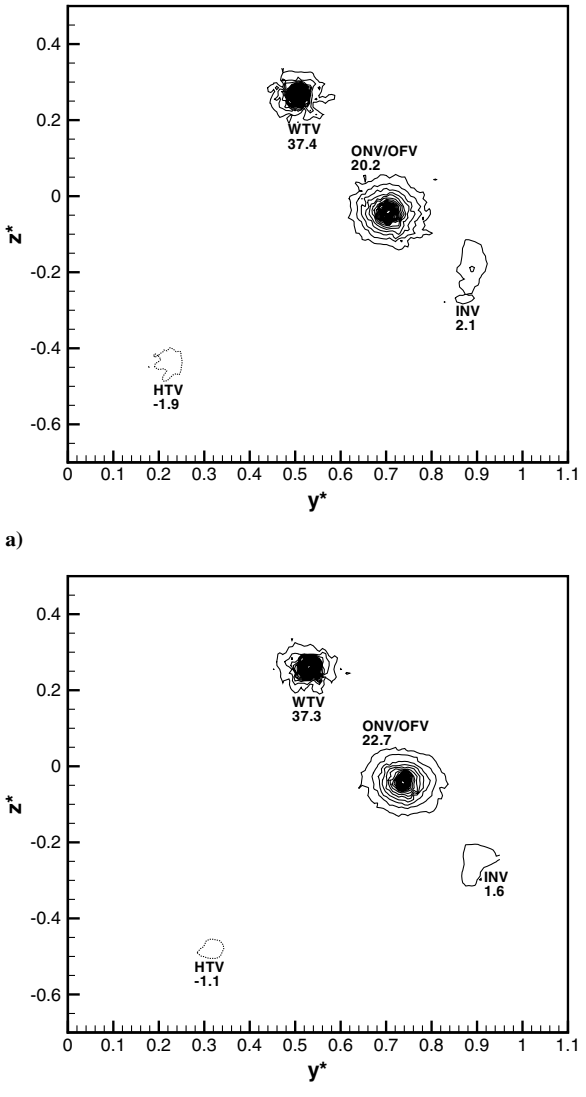


a)

b)

**Fig. 5 Contour plots of nondimensional axial vorticity $\xi$ distributions at $x^* = 4.7$ and $Re_{l_u} = 0.52 \times 10^6$ ($-20 \le \xi \le 50$ and $\Delta\xi = 1$) for the a) baseline configuration and b) configuration with landing gear; solid lines are positive values and dashed lines are negative values.**

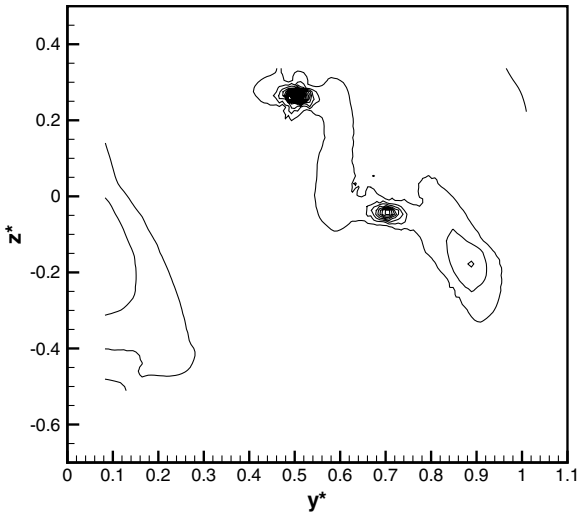


a)

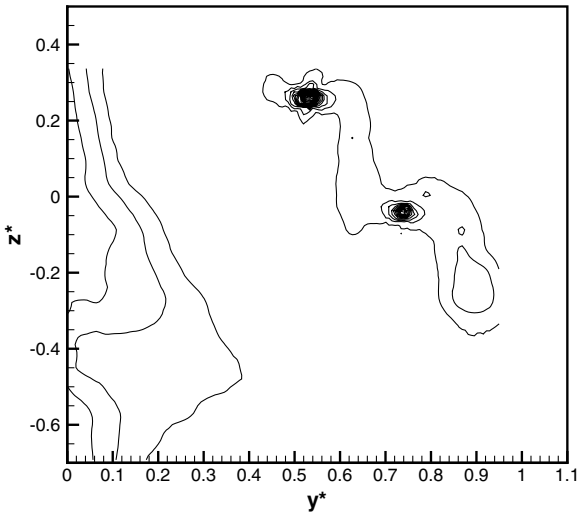


b)

**Fig. 6 Contour plots of turbulence intensity $Tu_y$ distributions at $x^* = 4.7$ and $Re_{l_\mu} = 0.52 \times 10^6$ ($0.02 \leq Tu_y \leq 0.2$ and $\Delta Tu_y = 0.01$) for the a) baseline configuration and b) configuration with landing gear.**

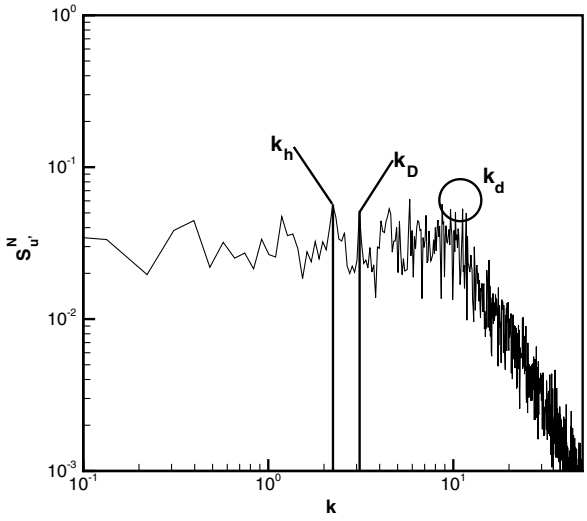


a)

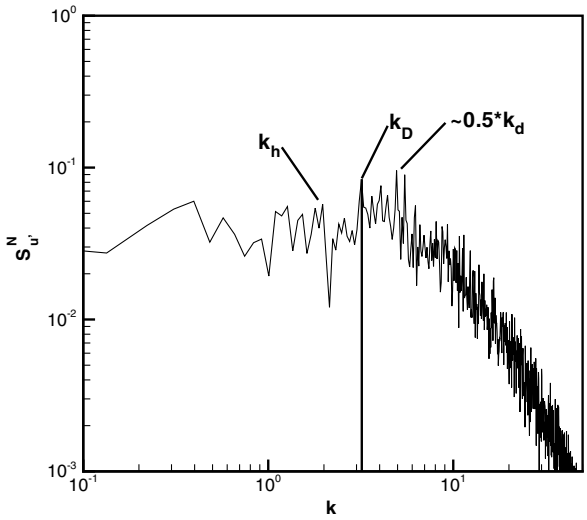


b)

**Fig. 7 Normalized power spectral densities of the axial velocity fluctuations at $x^* = 0.02$ for the configuration with landing gear; $Re_{l_\mu} = 0.52 \times 10^6$.**

by the landing gear is still clearly evident. Apart from the displacement effect, no major influence of the landing gear on the wake vortex roll-up process can be determined at $x^* = 4.7$.

Power spectral density distributions of the axial velocity fluctuations are evaluated. The spectral densities are calculated using a fast Fourier transformation of the velocity fluctuation time series, with a linear band-averaging based on 1024 frequency bands. The evaluation is performed to detect characteristic spectral peaks, indicating that turbulent kinetic energy is channeled into a narrow band due to quasi-periodic fluctuations.

The presence of instability mechanisms propagating along the wake vortex in the streamwise direction can lead to a relevant distortion of the vortex, accelerating its dispersion and decay [15]. Usually, long, medium, and short wave instabilities occur [16–19].

For the configuration with landing gear, the considered time series are taken from measurement positions located in the landing gear wake at $x^* = 0.02$ (Fig. 7). These positions are indicated in Fig. 2 by diamond symbols. Because the leading geometric parts of the landing gear are related to cylindrical elements, one may expect some frequency-dependent energy concentrations linked to periodic-vortex-shedding mechanisms. Characteristic length scales are given by $d = 0.019$ m (landing gear stay), $D = 0.1$ m (lateral extension of wheel pair), and $h = 0.13$ m (vertical extension of inclined wheels). A Strouhal number of $Sr = 0.2 \pm 0.1$ is attributed to periodic vortex shedding for the given Reynolds number range [$Re(l = d, D, h) = 0.28 - 1.9 \times 10^5$: laminar to transition]. Considering the velocity of $U_\infty = 25$ m/s, the corresponding reduced-frequency values are in the range of $k_d = 14.9$–$16.4$, $k_D = 2.8$–$3.2$, and $k_h = 2.2$–$2.4$. The landing gear wake spectra show some moderate energy concentrations at these reduced frequencies, but there is no significant increase in the power spectral densities. Further downstream at $x^* = 0.37$, the spectra exhibit broadband characteristics, the distributions of which are generally similar to those of the wing vortex sheet.

## Conclusions

An investigation on a LTA model is conducted for a typical landing configuration without and with main landing gear, addressing its influence on the wake roll-up process and the strength of dominating wake vortices and their positions. The landing gear consists of the stay and the four wheels, which are inclined with respect to the landing configuration investigated. The stay and the wheels create a bluff-body wake that interferes with the shear layer emanating from the wing and the wing–fuselage junction.

Therefore, compared with the baseline configuration, the flowfield features attributed to the deployed landing gear are as follows for near-field characteristics ($x^* = 0.02$–$1.0$):

1) The landing gear wake is associated with additional vorticity spots of moderate levels, forming a low-energy landing gear vortex system.

2) The landing gear wake is also indicated by an area of increased turbulence intensities, which is located within $0.12 < y^* < 0.25$ and $-0.1 < z^* < -0.3$ at $x^* = 0.02$. This area is shaped like an eight, which corresponds to the two inclined wheel pairs. The upper turbulence bubble refers to the inclined front wheel pair, the lower one to the inclined rear wheel pair. The vertical extension of the landing gear wake turbulence area is therefore about twice the lateral one, and the turbulence area of the wing vortex sheet also becomes expanded.

3) The spectral densities of the axial velocity fluctuations show generally broadband characteristics, with some peaks of moderate energy concentration attributed to coherent periodic structures of the landing gear wake. A strong energy concentration at specific frequencies cannot be detected.

4) At $x^* = 0.37$, the axial vorticity distribution still indicates the landing gear vortex system. Because of the wing downwash, the area of the landing gear wake turbulence moves downward, spreading out the whole area of high turbulence intensities in the wing–fuselage region. Again, the spectral densities exhibit a broadband behavior, with some moderate energy peaks that are similar to the ones for the wing vortex sheet.

5) The displacement effect of the landing gear wake shifts the vortex centers of the main vortices slightly outboard, and the horizontal tail plane vortex (HTV) shows a more noticeable outboard shift of about $\Delta y^* = 0.04$ at $x^* = 1.0$. The landing gear wake interference retards the roll-up process and, especially, the inboard movement of the HTV.

The extended near-field characteristics ($x^* = 1.0$–$4.7$) are as follows:

1) The landing gear wake interference continues to retard the inboard movement of the HTV. Downstream, the difference in the lateral HTV position reaches a value of $\Delta y^* \approx 0.1$ ($x^* = 4.7$).

2) The inboard areas of high turbulence intensities are further enlarged, clearly showing the annularly shaped region of the landing gear wake turbulence.

3) Despite the overall moderate outboard shift in vortex positions, the wake roll-up process is not markedly affected by the presence of the deployed landing gear. The main influence is attributed to the inboard region in which the area of high velocity fluctuations becomes significantly enlarged in the lateral and vertical directions.

Summarizing, the influence of the landing gear on the wake vortex is small. The strength and position of the wake vortices stay almost unchanged, and thus the impact on reducing aircraft separation distances is negligible.

## Acknowledgments

The support of this investigation within the Specific Targeted Research Project "FAR-Wake" of the Sixth Framework Programme of the European Union under contract AST4-CT-2005-012238 is gratefully acknowledged.

## References

[1] Donaldson, C. duP., and Bilanin, A. J., "Vortex Wakes of Conventional Aircraft," AGARD, AGARDograph No. 204, May 1975.

[2] Spalart, P. R., "Airplane Trailing Vortices," *Annual Review of Fluid Mechanics*, Vol. 30, 1998, pp. 107–138. doi:10.1146/annurev.fluid.30.1.107

[3] Gerz, T., Holzäpfel, F., and Darracq, D., "Commercial Aircraft Wake Vortices," *Progress in Aerospace Sciences*, Vol. 38, No. 3, 2002, pp. 181–208. doi:10.1016/S0376-0421(02)00004-0

[4] Elsenaar, A., "The Optimum Wing Load Distribution to Minimize Wake Vortex Hazard," *Conference on Capacity and Wake Vortices*, Imperial College London, London, Sept. 2001.

[5] Brenner, F., "Air Traffic Control Procedures for the Avoidance of Wake Vortex Encounters: Today and Future Developments by Deutsche Flugsicherung GmbH," *The Characterisation & Modification of Wakes from Lifting Vehicles in Fluids*, AGARD-CP-584, AGARD, Neuilly-sur-Seine, France, May 1996, pp. 4-1–4-14 .

[6] Hünecke, K., "Structure of a Transport Aircraft-Type Near Field Wake," *The Characterisation & Modification of Wakes from Lifting Vehicles in Fluids*, AGARD-CP-584, AGARD, Neuilly-sur-Seine, France, May 1996, pp. 5-1–5-9 .

[7] Hünecke, K., "From Formation to Decay—Extended-time Wake Vortex Characteristics of Transport-Type Aircraft," AIAA Paper 2002-3265, June 2002.

[8] Henke, R., "Validation of Wing Technologies on an Airbus A340 Flying Testbed: First Flight Test Results from the European Program AWIATOR," 24th Congress of the International Council of the Aeronautical Sciences, Yokohama, Japan, International Council of the Aeronautical Sciences, Paper ICAS-2004-4.4.1, Sept. 2004.

[9] Coustols, E., Stumpf, E., Jacquin, L., Moens, F., Vollmers, H., and Gerz, T., "Minimised Wake: A Collaborative Research Programme on Aircraft Wake Vortices," AIAA Paper 2003-0938, Jan. 2003.

[10] Crouch, J. D., Miller, G. D., and Spalart, P. R., "Active-Control System for Breakup of Airplane Trailing Vortices," *AIAA Journal*, Vol. 39, No. 12, 2001, pp. 2374–2381.

[11] Allen, A., and Breitsamter, C., "Influence of Wing Elements on Large Transport Aircraft Wake," Technical Univ. of Munich, TR TUM-AER-2007/7, Munich, 2007.

[12] Breitsamter, C., "Turbulente Strömungsstrukturen an Flugzeugkonfigurationen mit Vorderkantenwirbeln," Dissertation, Technical Univ. of Munich, Herbert Utz Verlag Wissenschaft (Aerodynamik), Munich, June 1997.

[13] Breitsamter, C., Bellastrada, C., and Laschka, B., "Investigations on the Turbulent Wake Vortex Flow of Large Transport Aircraft," *23rd International Congress of the Aeronautical Sciences*, International Council of the Aeronautical Sciences, Reston, VA, Sept. 2002, pp. 382.1–382.13.

[14] Hünecke, K., "The Characterisation of Transport Aircraft Vortex Wakes," AIAA Paper 2001-2427, June 2001.

[15] Jacquin, L., Fabre, D., Sipp, D., Theofilis, V., and Vollmers, H., "Instabilities and Unsteadiness of Aircraft Wake Vortices," *Aerospace Science and Technology*, Vol. 7, No. 8, 2003, pp. 577–593. doi:10.1016/j.ast.2003.06.001

[16] Crow, S. C., "Stability Theory for a Pair of Trailing Vortices," *AIAA Journal*, Vol. 8, No. 12, 1970, pp. 2172–2179.

[17] Crouch, J. D., "Instability and Transient Growth for Two Trailing-Vortex Pairs," *Journal of Fluid Mechanics*, Vol. 350, 1997, pp. 311–330. doi:10.1017/S0022112097007040

[18] Breitsamter, C., "Nachlaufwirbelsysteme großer Transportflugzeuge—Experimentelle Charakterisierung und Beeinflussung," Habilitationsschrift, Technical Univ. of Munich, Herbert Utz Verlag (Aerodynamik), Munich, Feb. 2007.

[19] Meunier, P., and Leweke, T., "Three-Dimensional Instability During Vortex Merging," *Physics of Fluids*, Vol. 13, No. 10, 2001, pp. 2747–2750. doi:10.1063/1.1399033